Perfect spin filtering controlled by an electric field in a bilayer graphene junction: Effect of layer-dependent exchange energy*

Kitakorn Jatiyanon[1], I-Ming Tang[2], and Bumned Soodchomshom[1,†]

[1] Department of Physics, Faculty of Science, Kasetsart University, Bangkok 10900, Thailand
[2] Department of Materials Science, Faculty of Science, Kasetsart University, Bangkok 10900, Thailand

(Received 11 January 2016; revised manuscript received 26 February 2016; published online 31 May 2016)

Magneto transport of carriers with a spin-dependent gap in a ferromagnetic-gated bilayer of graphene is investigated. We focus on the effect of an energy gap induced by the mismatch of the exchange fields in the top and bottom layers of an AB-stacked graphene bilayer. The interplay of the electric and exchange fields causes the electron to acquire a spin-dependent energy gap. We find that, only in the case of the anti-parallel configuration, the effect of a magnetic-induced gap will give rise to perfect spin filtering controlled by the electric field. The resolution of the spin filter may be enhanced by varying the bias voltage. Perfect switching of the spin polarization from $+100\%$ to -100% by reversing the direction of electric field is predicted. Giant magnetoresistance is predicted to be easily realized when the applied electric field is smaller than the magnetic energy gap. It should be pointed out that the perfect spin filter is due to the layer-dependent exchange energy. This work points to the potential application of bilayer graphene in spintronics.

Keywords: bilayer graphene, spin filter, magnetoresistance, spintronics

PACS: 81.05.ue, 72.80.Vp, 72.25.–b, 73.43.Qt **DOI:** 10.1088/1674-1056/25/7/078104

1. Introduction

Monolayer graphene[1] has become a promising material for applications in nanoelectronics such as in high speed transistors[2,3] and spintronics.[4] This is due to its intriguing electronic properties.[5] Monolayer graphene can be considered as a gapless semiconductor; its carriers mimic two-dimensional massless Dirac fermions with the speed of light replaced by the Fermi velocity $v_F \approx 10^6$ m/s. The mass of the Dirac fermion in graphene acts as the energy gap. The wave functions of electrons in A- and B-sublattices play the role of pseudo-spin $\uparrow$ and pseudo-spin $\downarrow$ states, respectively. Electrons in graphene also have a valley degree of freedom k and k' different from those of 3-dimensional Dirac fermions in a vacuum. Because of its carrier behaving like a relativistic particle, graphene could be considered as a high energy system in condensed matter.[6] Massless Dirac fermion in graphene can tunnel through the electric-gated barrier without back reflection at the normal incident, which is called "Klein tunneling".[7] This effect arises from the conservation of the chirality. It is therefore difficult for a gapless graphene-based field effect transistor to suppress the current for off-state by an electric gate control. In general, graphene is non-magnetic but it can be induced into a ferromagnetic state by means of the proximity effect.[8–12] This property is very important for application of graphene in spintronic technology.[4] A lot of attention[13–17] has been given to magnetotransport in monolayer graphene-ferromagnetic junctions. Spin polarization and magnetoresistance in monolayer graphene nanoribbon[17] was investigated. It has also been found that the interplay of ferromagnetism and strain leads to controllable spin-valley currents.[18–20]

Bilayer graphene has some properties that are different from those of monolayer graphene. One of them is the opening of the gap by an applied electric field.[21,22] When the potential energies $V_{1(2)}$ of the electrons in layer 1 (2) are different, the gap opening in AB-stacked bilayer graphene is given by $E_{\rm gap} = (V_2 - V_1)/2$.[21] Monolayer graphene lacks this property since its atomic structure is planar. Due to the differences, transport in bilayer graphene leads to different behavior from those of the monolayer graphene such as anti-Klein tunneling (or perfect back reflection) at the normal incidence.[23] The current in the bilayer graphene junction can be suppressed easily by an electric gate. Similar to monolayer graphene, bilayer graphene can be induced into the ferromagnetic state by means of the proximity effect.[24–31] Magnetoresistance and spin polarization in bilayer graphene have been investigated.[24–26,31] The magnetism in bilayer under the influence of pressure has also been studied.[27] Experimental study of quantum Hall ferromagnetism in bilayer graphene was recently completed.[30]

In this paper, we will investigate the effect of layer-dependent ferromagnetism on the magnetotransport property in an AB-stacked bilayer graphene-based N/F/N junction, where N and F are normal and ferromagnetic regions, respectively. We would take the exchange energy in the top layer to be different from that in the bottom layer in the barrier region in the junction. Through this means, the energy gap of the electron in the barrier junction will become spin-dependent when an electric field is applied. This property will be described in the theoretical model. The effect of the interplay

*Project supported by the Kasetsart University Research and Development Institute (KURDI) and Thailand Research Fund (TRF) (Grant No. TRG5780274).
†Corresponding author. E-mail: Bumned@hotmail.com; fscibns@ku.ac.th
© 2016 Chinese Physical Society and IOP Publishing Ltd

of electric and exchange fields on the spin transport property is the main focus of our work, which had not been clarified in previous studies.[25,26,29,31] This effect does not appear in a monolayer graphene ferromagnetic junction.[8,32] Our work aims to show the potential of layer-dependent ferromagnetism in bilayer graphene, which can generate the carriers with spin-dependent gap controlled by electric field for application in spintronics.

2. Hamiltonian model

The model of our proposed NFN junction, where N represents a normal bilayer graphene region and F represents a ferromagnetic bilayer graphene region, is depicted in Fig. 1(a). To achieve the latter region, two magnetic insulators are placed above and below a narrow strip of bilayer graphene so that each insulator is in contact with either the top or bottom layer of the bilayer graphene. The proximity effect will induce an exchange field in the graphene sandwiched between the two insulators and will induce the graphene into a ferromagnetic state. This would be the ferromagnetic barrier region (of thickness L) in our NFN bilayer graphene junction. Depending on the direction of the magnetism in the two insulators, two configurations are possible leading to parallel (P) and antiparallel (AP) junctions. The P-(AP-) junction corresponds to the top and bottom exchange fields being parallel (anti-parallel). The gate potential $-U/e$ and perpendicular electric field E_z can also be imposed on the junction. The magnitude of exchange energy "h" induced by the two magnetic insulators in both layers is assumed to have the same value. The wave function of the electron in bilayer graphene will be in the form of a four-state component wave function $\psi = \left(\begin{array}{cccc}\varphi_{A1} & \varphi_{B1} & \varphi_{A2} & \varphi_{B2}\end{array}\right)^{T}$, where 1(2) and A (B) denote the top (bottom) layer and the sublattice A (B), respectively.

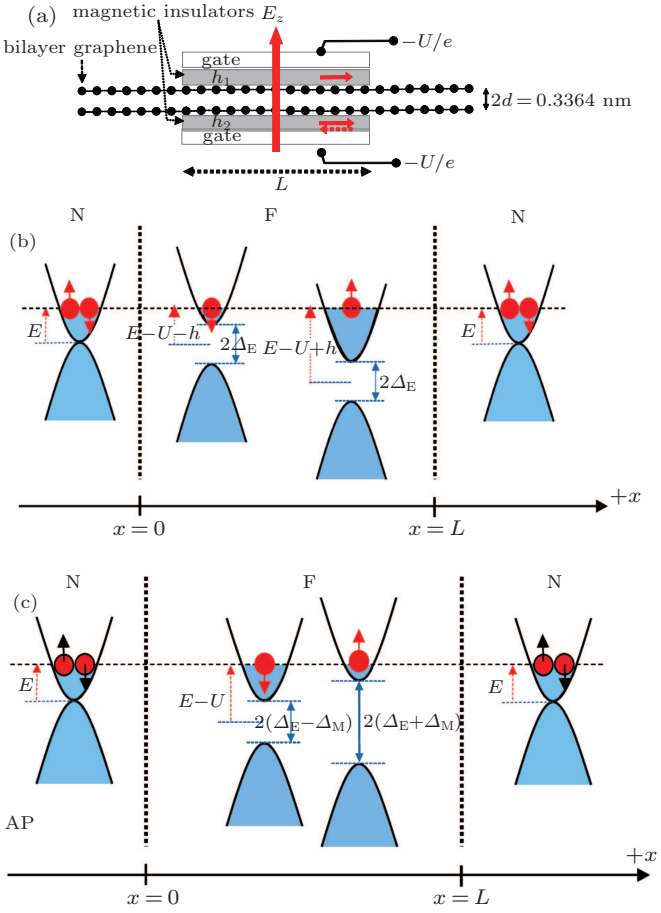


Fig. 1. (color online) Schematic illustration of bilayer graphene-based normal/ferromagnetic/normal junction (a) where h_1 and h_2 are the exchange energies in the top and bottom layers, respectively. The spin-dependent energy levels in each region of the P-junction and spin-dependent energy levels in each region of the AP-junction are illustrated in panels (b) and (c), respectively. In the case of $|h_1| = |h_2| = h = \Delta_M$, the spin-dependent gap is generated only when the junction is an AP-junction and there is no spin splitting.

The Hamiltonian for electrons in the barrier region of the AB-stacked bilayer graphene ferromagnetic junction[21,33] in the P-(AP-) configuration is

$$\hat{H}_{\sigma,\mathrm{P(AP)}} = \begin{pmatrix} eE_zd-\sigma h & \hat{\pi}^* & 0 & 0 \\ \hat{\pi} & eE_zd-\sigma h & t & 0 \\ 0 & t & -eE_zd-(+)\sigma h & \hat{\pi}^* \\ 0 & 0 & \hat{\pi} & -eE_zd-(+)\sigma h \end{pmatrix} + U\hat{I}_{4\times4}, \tag{1}$$

where $\pi^* = \hbar v_F(\hat{k}_x - \mathrm{i}\hat{k}_y)$, t is the interlayer hopping energy, and $\hat{I}_{4\times4}$ is the unit matrix. In the above, $\sigma = 1(-1)$ for spin $\uparrow(\downarrow)$, and d is the distance between the top and bottom layers. At low energy, the P- and AP-Hamiltonian reduces to the following two component Hamiltonians acting on the pseudo spinor $\psi_\sigma = \left(\begin{array}{cc}\varphi_{A1,\sigma} & \varphi_{B2,\sigma}\end{array}\right)^{T}$ as

$$\hat{H}_{\mathrm{F,P}} = \begin{pmatrix} \Delta_E & -\frac{\hbar^2}{2m}\left(\hat{k}_x - \mathrm{i}\hat{k}_y\right)^2 \\ -\frac{\hbar^2}{2m}\left(\hat{k}_x + \mathrm{i}\hat{k}_y\right)^2 & -\Delta_E \end{pmatrix} + (U-\sigma h)\hat{I}_{2\times2}, \tag{2}$$

$$\hat{H}_{\mathrm{F,AP}} = \begin{pmatrix} (\Delta_E+\sigma h) & -\frac{\hbar^2}{2m}\left(\hat{k}_x - \mathrm{i}\hat{k}_y\right)^2 \\ -\frac{\hbar^2}{2m}\left(\hat{k}_x + \mathrm{i}\hat{k}_y\right)^2 & -(\Delta_E+\sigma h) \end{pmatrix} + U\hat{I}_{2\times2}, \tag{3}$$

where $\Delta_E = eE_zd$ is the electric field-induced gap, $\hat{k}_{x(y)} = -\mathrm{i}\partial_{x(y)}$ is the wave vector operator, $\hat{I}_{2\times2}$ is the unit matrix, and $m = t/2v_F^2 \cong 0.054m_e$[31] is the effective mass with m_e being electron bare mass. The effective Hamiltonian for the elec-

trons in the normal region (N) is obtained by setting $h = 0$, $U = 0$, and $\Delta_{\rm E} = 0$ in Eq. (2) or (3),[6,21] and is

$$\hat{H}_{\rm N,P(AP)} = \begin{pmatrix} 0 & -\frac{\hbar^2}{2m}\left(\hat{k}_x - {\rm i}\hat{k}_y\right)^2 \\ -\frac{\hbar^2}{2m}\left(\hat{k}_x + {\rm i}\hat{k}_y\right)^2 & 0 \end{pmatrix}. \quad (4)$$

In the barrier, the spin-dependent Eigen energies for the Hamiltonian for P- and AP-junctions in Eqs. (2) and (3) are, respectively,

$$E = \pm\sqrt{\left(\frac{p_{\rm P}^2}{2m}\right)^2 + \Delta_{\rm E}^2} + U - \sigma h, \quad (5)$$

$$E = \pm\sqrt{\left(\frac{p_{\rm AP}^2}{2m}\right)^2 + (\Delta_{\rm E} + \sigma h)^2} + U. \quad (6)$$

For the N-regions,

$$E = \pm\frac{q^2}{2m}. \quad (7)$$

Here, p and q represent momentums in F and N regions, respectively and E is the energy of the electron.

In the normal region, the bilayer graphene becomes a gapless semiconductor. The energy levels for spin up and down electrons in each region are described in Fig. 1(b). The exchange fields in the P-junction generate the spin-splitting. The energy gap $\varepsilon_{{\rm P},\sigma} = 2|\Delta_{\rm E}|$ of electron in the P-junction is generated solely by the electric field. The junction leads to magnetic-induced gap $\Delta_{\rm M} = h$ only in the case of the AP-junction. This is due to the mismatch of exchange fields in the top and bottom layers in the barrier region. The spin-dependent energy gap in the AP-junction has the form

$$\varepsilon_{{\rm AP},\sigma} = 2\left|\Delta_{\rm E} + \sigma\Delta_{\rm M}\right|. \quad (8)$$

As we have seen in Eq. (8), for $\Delta_{\rm E} = \Delta_{\rm M}$, the electron with spin $\uparrow$ acquires an energy gap of $2\Delta_{\rm M}$, while the electron with spin $\downarrow$ will be gapless. The strong differences in energy gaps of spin-up and spin-down electrons in the AP-junction would give rise to an intriguing magnetotransport property.

3. Scattering process

In this section, we study the scattering process in an AB-stacked bilayer graphene-based N/F/N junction. The current is taken to flow in the x direction. The wave functions of the carriers in the system are combinations of the eigen solutions of the two-component Hamiltonian defined by Eqs. (2)–(4). If the electrons are being injected at an angle θ to the plane of the interface between the different regions of the junction, the momentum in the y direction will be conserved and is given by $k_{||} = \sqrt{2m|E|}\sin\theta/\hbar$ with E being the excitation energy. The wave functions of the electrons in the left-N, and right-N for the P and AP cases are

$$\psi_{\rm N(L)} = \left[\begin{pmatrix} 1 \\ -{\rm e}^{2{\rm i}\theta} \end{pmatrix} {\rm e}^{{\rm i}k_{\rm N}x} + r\begin{pmatrix} 1 \\ -{\rm e}^{-2{\rm i}\theta} \end{pmatrix} {\rm e}^{-{\rm i}k_{\rm N}x} + r'\begin{pmatrix} 1 \\ \beta_+ \end{pmatrix} {\rm e}^{q_{\rm N}x}\right] {\rm e}^{{\rm i}k_{||}y},$$

$$\psi_{\rm N(R)} = \left[t\begin{pmatrix} 1 \\ -{\rm e}^{2{\rm i}\theta} \end{pmatrix} {\rm e}^{{\rm i}k_{\rm N}x} + t'\begin{pmatrix} 1 \\ \beta_- \end{pmatrix} {\rm e}^{-q_{\rm N}x}\right] {\rm e}^{{\rm i}k_{||}y}, \quad (9)$$

where

$$\beta_\pm = \frac{\hbar^2\left(q_{\rm N}mk_{||}\right)^2}{2mE}, \quad k_{\rm N} = \sqrt{2m|E|}\cos\theta/\hbar,$$

with $q_{\rm N} = \sqrt{2m|E|/\hbar^2 + k_{||}^2}$. The reflected and transmitted coefficients are r and t, respectively while the amplitudes of decaying states in the left-N region and the right-N region are r' and t', respectively.

The wave function in the ferromagnetic barrier of a P-junction is given by

$$\psi_{\rm F,P} = \left[a_{2,\rm P}\begin{pmatrix} \gamma_{\rm P}{\rm e}^{-2{\rm i}\varphi_{\rm P}} \\ 1 \end{pmatrix} {\rm e}^{{\rm i}k_{\rm P}x} + a_{1,\rm P}\begin{pmatrix} \gamma_{\rm P}{\rm e}^{2{\rm i}\varphi_{\rm P}} \\ 1 \end{pmatrix} {\rm e}^{-{\rm i}k_{\rm P}x} + b_{2,\rm P}\begin{pmatrix} \eta_{2,\rm P} \\ 1 \end{pmatrix} {\rm e}^{q_{\rm P}x} + b_{1,\rm P}\begin{pmatrix} \eta_{1,\rm P} \\ 1 \end{pmatrix} {\rm e}^{-q_{\rm P}x}\right] {\rm e}^{{\rm i}k_{||}y}, \quad (10)$$

where

$$\gamma_{\rm P} = \frac{\hbar^2 k_{\rm F,P}^2}{2m\left(\Delta_{\rm E} + U - \sigma h - E\right)},$$

$$\eta_{1,\rm P} = -\frac{\hbar^2\left(q_{\rm P} - k_{||}\right)^2}{2m\left(\Delta_{\rm E} + U - \sigma h - E\right)},$$

$$\eta_{2,\rm P} = -\frac{\hbar^2\left(q_{\rm P} + k_{||}\right)^2}{2m\left(\Delta_{\rm E} + U - \sigma h - E\right)},$$

$$k_{\rm P} = \sqrt{\frac{2m}{\hbar^2}\sqrt{(E - U + \sigma h)^2 - (\Delta_{\rm E})^2} - k_{||}^2},$$

$$q_{\rm P} = \sqrt{\frac{2m}{\hbar^2}\sqrt{(E - U + \sigma h)^2 - (\Delta_{\rm E})^2} + k_{||}^2},$$

and $\varphi_{\rm P} = \sin^{-1}\left(k_{||}/k_{\rm F,P}\right)$ with

$$k_{\rm F,P} = \sqrt{\frac{2m}{\hbar^2}\sqrt{(E - U + \sigma h)^2 - (\Delta_{\rm E})^2}}. \quad (11)$$

The wave function in the ferromagnetic barrier of an AP-junction is obtained by changing the subscripted notation P $\rightarrow$ AP, where the coefficients are now

$$\gamma_{\rm AP} = \frac{\hbar^2 k_{\rm F,AP}^2}{2m\left(\Delta_{\rm E} - \sigma\Delta_{\rm M} + U - E\right)},$$

$$\eta_{1,\rm AP} = -\frac{\hbar^2\left(q_{\rm AP} - k_{||}\right)^2}{2m\left(\Delta_{\rm E} - \sigma\Delta_{\rm M} + U - E\right)},$$

$$\eta_{2,\rm AP} = -\frac{\hbar^2\left(q_{\rm AP} + k_{||}\right)^2}{2m\left(\Delta_{\rm E} - \sigma\Delta_{\rm M} + U - E\right)},$$

$$k_{\rm AP} = \sqrt{\frac{2m}{\hbar^2}\sqrt{(E - U)^2 - (\sigma\Delta_{\rm M} - \Delta_{\rm E})^2} - k_{||}^2},$$

$$q_{\rm AP} = \sqrt{\frac{2m}{\hbar^2}\sqrt{(E - U)^2 - (\sigma\Delta_{\rm M} - \Delta_{\rm E})^2} + k_{||}^2},$$

and $\varphi_{\rm AP} = \sin^{-1}\left(k_{||}/k_{\rm F,AP}\right)$ with

$$k_{\rm F,AP} = \sqrt{\frac{2m}{\hbar^2}\sqrt{(E-U)^2 - (\sigma\Delta_{\rm M} - \Delta_{\rm E})^2}}. \quad (12)$$

All amplitudes of the wave function or coefficients r, r', t, t', $a_{1,2}$, and $b_{1,2}$ in Eqs. (9) and (10) can be determined by matching the wave functions at the interfaces located at $x = 0$ and $x = L$, i.e., by requiring that at the two interfaces

$$\begin{aligned}
&\psi_{\rm N(L)}(x \to 0^-) = \psi_{\rm F}(x \to 0^+),\\
&\partial_x\psi_{\rm N(L)}(x \to 0^-) = \partial_x\psi_{\rm F}(x \to 0^+),\\
&\psi_{\rm F}(x \to L^-) = \psi_{\rm N(R)}(x \to L^+),\\
&\partial_x\psi_{\rm F}(x \to L^-) = \partial_x\psi_{\rm N(R)}(x \to L^+). \quad (13)
\end{aligned}$$

The transmitted coefficient in the case of the P (AP) junction is given by $t \to t_{\rm P(AP)}$ in Eq. (9) corresponding to the P (AP) type.

4. Transport formulae

The current density in the x direction is given by

$$J = \frac{{\rm i}\hbar}{2m}\left[(\psi^*\sigma_x\partial_x\psi) - (\partial_x\psi^*\sigma_x\psi) + 2(\psi^*\sigma_y\partial_y\psi)\right],$$

where $\sigma_{x(y)}$ is the Pauli spin matrix in the $x(y)$ direction and ψ are the wave functions for the electrons in the different regions of the junction. For the AB-stacked bilayer graphene ferromagnetic junction[21,33] in either the P or AP configuration, the wave equations are given by Eqs. (9)–(12). Using the above expression and wave functions, and neglecting the decaying amplitude, we will obtain the following transmission through the junction:

$$T_{\uparrow,\downarrow}(\theta) = \left(J_{\rm tran}/J_{\rm inject}\right)_{\uparrow,\downarrow} = (t^*t)_{\uparrow,\downarrow}, \quad (14)$$

where $J_{\rm tran}$ and $J_{\rm inject}$ are calculated from the transmitted and injected wave functions, respectively. To simplify, we will next let $\xi = {\rm P}$ (AP) for the case of the P (AP) junction. Based on the standard Landauer's formalism,[34] the dimensionless spin-conductance formula is given as

$$G_{\xi,(\uparrow,\downarrow)} = \frac{1}{2}\int_0^{\pi/2} T_{\varsigma,(\uparrow,\downarrow)}(\theta)\cos\theta\,{\rm d}\theta. \quad (15)$$

The total conductance is defined as

$$G_\xi = G_{\xi,\uparrow} + G_{\xi,\downarrow}. \quad (16)$$

The spin polarization in the junction is defined by the ratio of the difference between the conductance of spin-up and spin-down currents, as given by

$$S_\xi = 100\% \times \left(G_{\xi,\uparrow} - G_{\xi,\downarrow}\right)/\left(G_{\xi,\uparrow} + G_{\xi,\downarrow}\right). \quad (17)$$

The tunneling magnetoresistance (TMR) of the junction is defined as

$${\rm TMR} = 100\% \times (G_{\rm P} - G_{\rm AP})/G_{\rm P}. \quad (18)$$

5. Result and discussion

In the numerical calculation, the ferromagnetism in bilayer graphene is assumed to be proximity-induced by magnetic insulators of exchange energy h =5 meV.[8] The thickness of the barrier L is taken to be 100 nm. We first study the spin-dependent transmissions for P and AP configurations, which are plotted in Fig. 2. In the case of no electric field-induced gap $\Delta_{\rm E} = 0$, the transmissions for two configurations are seen in Figs. 2(a) and 2(b). In this case, the carriers are gapless particles. The transmission of the AP-junction is not spin-dependent because there is no spin-dependent gap and exchange-induced-spin-splitting (see Fig. 2(b)). The spin-dependent transmission in the P-junction arisen explicitly from the exchange-induced-spin-splitting (see Fig. 2(a)). When an electric field is applied $\Delta_{\rm E} = h$, a strong spin-dependent gap $E_{\rm gap\uparrow} = 2h$ and $E_{\rm gap\downarrow} = 0$ occurs in the case of the AP-junction. This gives rise to a strong insulating barrier for the spin-$\uparrow$ electron but to a good conducting barrier for the spin-$\downarrow$ electron (see Fig. 2(d)). Electrons in the P-junction acquire the same energy gap $E_{\rm gap\uparrow,\downarrow} = 2\Delta_{\rm E}$, but at a different Fermi level. This would cause a different transmission of the electrons (see Fig. 2(c)). It can be concluded that the spin-dependent transmission in P- and AP-junctions is generated in different ways. In the P-junction, the spin-dependent transmission is generated by an exchange-field induced shift of the Fermi level $\mu_\uparrow \neq \mu_\downarrow$ with $\mu_\sigma = \sigma h - U$, just like a Zeeman splitting. In the case of the AP-junction, the spin-dependent transmission is due to the exchange-field effect on the spin-dependent-gap, which causes $E_{\rm gap\uparrow} \neq E_{\rm gap\downarrow}$, since $E_{{\rm gap},\sigma} = \Delta_{\rm E} + \sigma h$.

We next study the dependence of the spin-conductance $G_{\uparrow,\downarrow}$ on the electric field $\Delta_{\rm E} = eE_z d$ for both the P and AP configurations with $E = U$ in Fig. 3. As seen in Figs. 3(b) and 3(d), the perfect spin filter, (i.e. the spin conductance splits into two peaks perfectly) occurs when the junction is anti-parallel. This behavior is stable under a varying $E \gg h$. The P-junction does not exhibit such behavior. The junction exhibits a strong conducting junction when E is inside the interval $-h \leq \Delta_{\rm E} \leq +h$, as plotted in Figs. 3(a) and 3(c). In Fig. 4, we show that there is no spin-conductance splitting in the P-junction, even when varying $U \neq E$. For Δ_E is in the interval $-|E+h-U| \leq \Delta_{\rm E} \leq |E+h-U|$, a spin-up electron will flow through the junction, while a spin-down electron will flow in the junction when Δ_E is in the interval $-|E-h-U| \leq \Delta_{\rm E} \leq |E-h-U|$. In Fig. 5, we see that an AP- junction with a perfect spin filter having a smaller spin-current band width is possible when $E = U$ (see Fig. 5(c)). This result points to the condition needed for an AP junction to exhibit the perfect spin filtering effect, which can be controlled by an electric field.

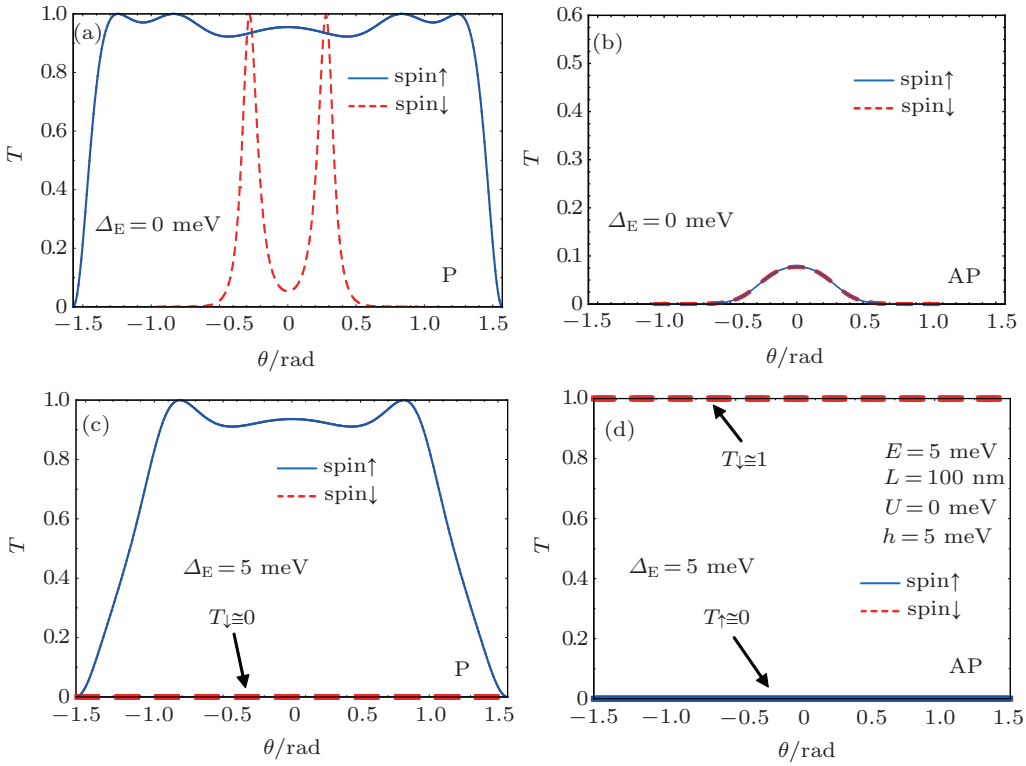


Fig. 2. (color online) Comparison of transmissions in the P and AP configurations at zero gate potential. P-and AP-junctions. Panels (a) and (b) show the transmissions for the two configurations when the electric field is absent (i.e., when $\Delta_E = 0$). Panels (c) and (d) show the transmission for the P and AP configurations in the presence of an electric field (i.e., $\Delta_E = h \neq 0$) respectively. Spin-dependent transmissions occur when the electric field and exchange field are applied in the magnetic AP-junction, $\Delta_E \neq 0$ and $h \neq 0$.

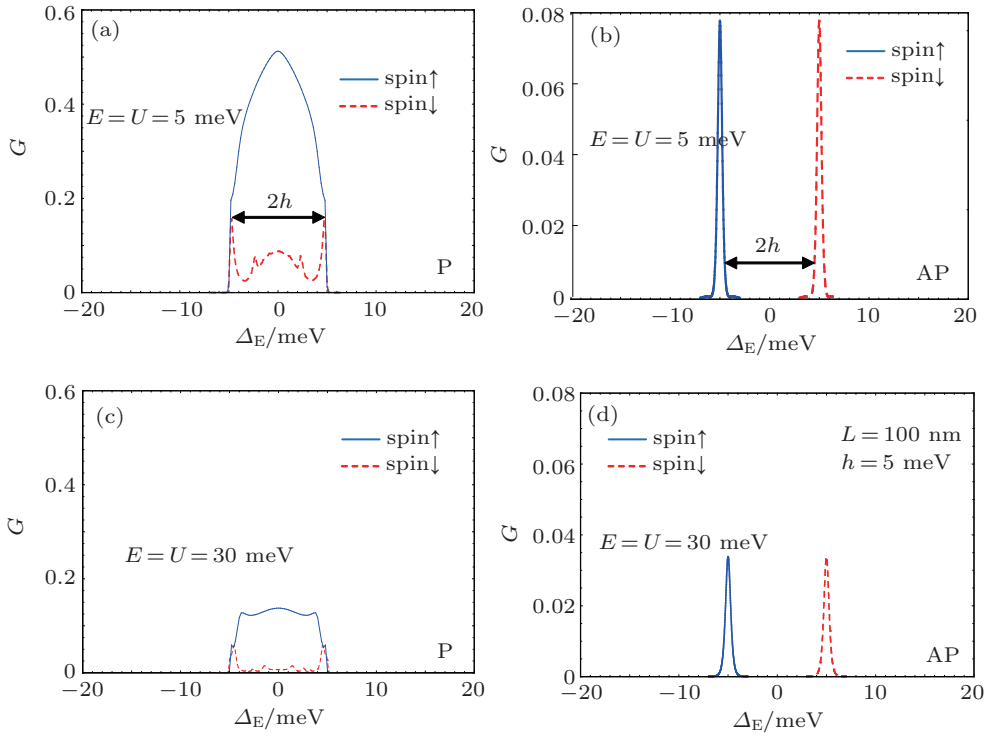


Fig. 3. (color online) Plot of spin conductance versus electric field-induced gap Δ_E in the case of (a) a P-junction with $E = U = 5$ meV, (b) an AP-junction with $E = U = 5$ meV, (c) a P-junction with $E = U = 30$ meV, and (d) an AP-junction with $E = U = 30$ meV, respectively. As is seen, the perfect (or complete) spin filter by varying electric field occurs only for the AP configuration.

The spin polarizations for the P- and AP-configurations are shown in Fig. 6. Interestingly, the behavior of the spin polarizations in the P-junction is quite different from that of the AP junction. It is seen that, the spin polarization in the P-junction, S_P, oscillates strongly above the zero point for $U \ll E$. For $U \gg E$, S_P oscillates below the zero point. At $U = E$, S_P oscillates about

the zero point. In contrast to that in the P-junction, S_{AP} in an AP junction exhibits perfect spin-polarization switching, instead of oscillating. Switching of spin polarization from +100% to −100% occurs when the electric field is reversed (remembering that $\Delta_E = eE_z d$).

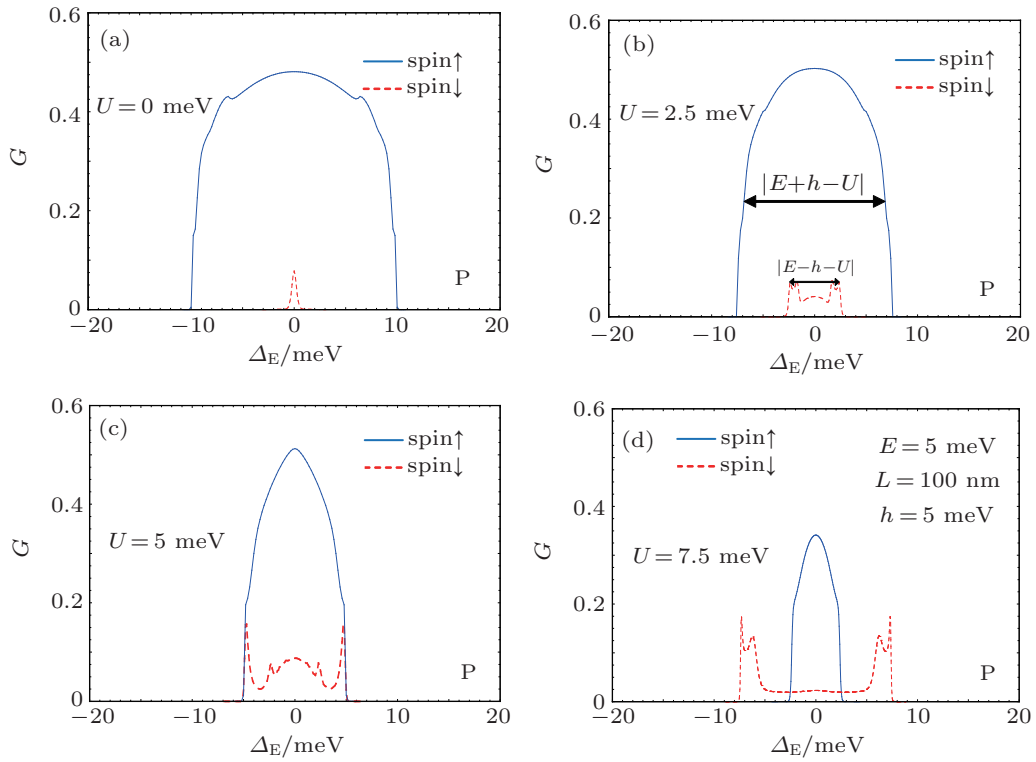


Fig. 4. (color online) Plot of spin conductance versus electric field-induced gap Δ_E in the case of $E = h = 5$ meV, for the P-junction with different values of U: (a) 0 meV, (b) 2.5 meV, (c) 5 meV, and (d) 7.5 meV.

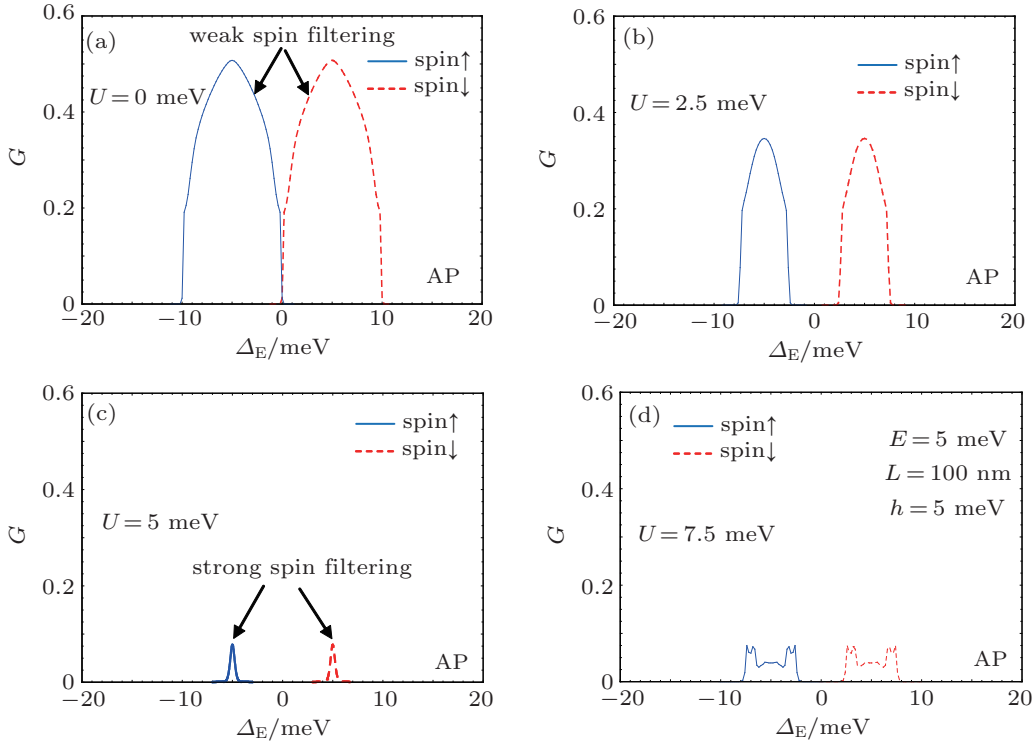


Fig. 5. (color online) Plot of spin conductance versus electric field-induced gap Δ_E in the case of $E = h = 5$ meV, for the AP-junction with different values of U: (a) 0 meV, (b) 2.5 meV, (c) 5 meV, and (d) 7.5 meV.

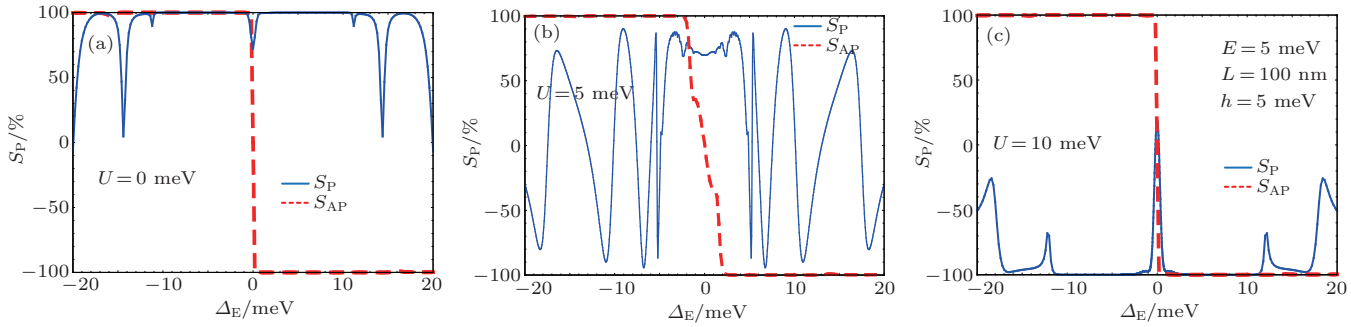


Fig. 6. (color online) Plot of spin polarization versus electric field-induced gap Δ_E in the case of $E = h$ for different values of U: (a) 0 meV, (b) 5 meV, and (c) 10 meV, respectively. The $S_{P(AP)}$ represents spin polarization of the P-(AP-) junction. Perfect switching of spin polarization from +100% to −100% controlled by electric field is predicted only in the AP-junction.

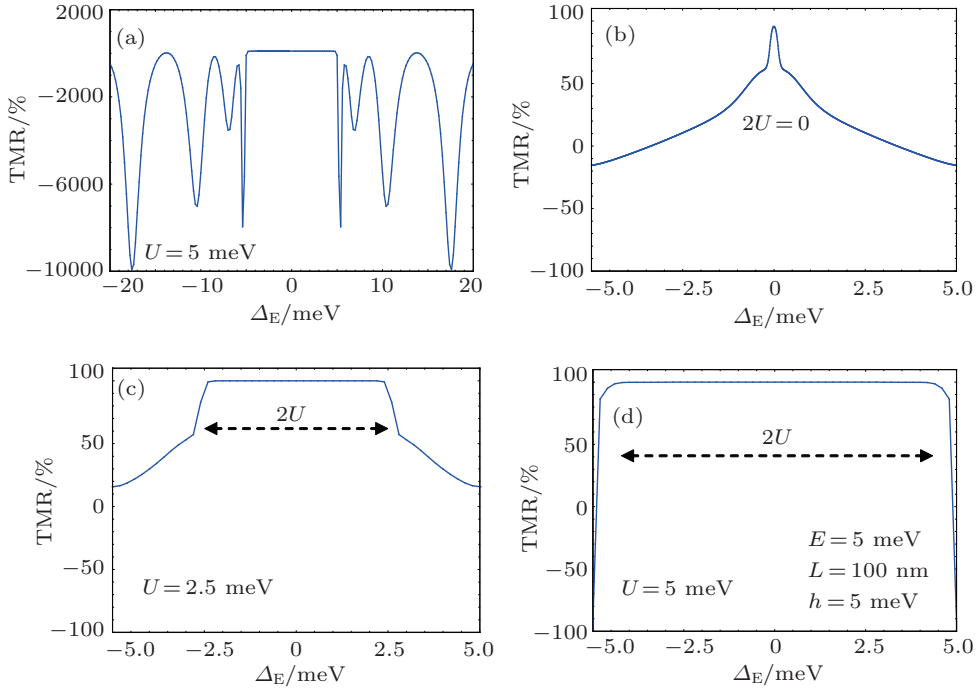


Fig. 7. (color online) Tunneling magnetoresistance (TMR) as a function of electric field-induced gap Δ_E in the case of $E = h = 5$ meV for (a) $U = 5$ meV, −20 meV< Δ_E < +20 meV, (b) $U = 0$, −54 meV< Δ_E < +5 meV, (c) $U = 2.5$ meV, −5 meV< Δ_E < +5 meV, and (d) $U = 5$ meV, −5 meV< Δ_E < +5 meV. The condition with the most stability for TMR=100% under a varying electric field is found at $E = h = U$.

Figure 7 shows that the TMR of the junction will oscillate as a function of Δ_E when Δ_E is in the interval of $-h \geq \Delta_E \geq h$ (with $U = E = h$), but a 100% TMR occurs when Δ_E is in the range of $-h \leq \Delta_E \leq h$ (see Figs. 7(a) and 7(d)). The TMR = 100% for arbitrary $U \leq h$ is predicted to occur in the range of $-U \leq \Delta_E \leq U$ (see Figs. 7(b)–7(d). The result will be clarified by considering the approximated momentums of electrons in P- and AP- barriers

$$k_{F,P} \cong \sqrt{\frac{2m}{\hbar^2}\sqrt{(E - U + \sigma h)^2 - (\Delta_E)^2}},$$

$$k_{F,AP} \cong \sqrt{\frac{2m}{\hbar^2}\sqrt{(E - U)^2 - (\sigma\Delta_M - \Delta_E)^2}}.$$

For $E = U = h$ (see Figs. 7(a) and 7(d)), we have $k_{F,P} = \sqrt{2m\sqrt{h^2 - \Delta_E^2}}/\hbar$. This causes the P-junction to become a good conductor having $G_P \gg 0$ when $-h \leq \Delta_E \leq h$. This condition also gives rise to the AP-junction becoming a strong insulator since $k_{F,AP} = i\sqrt{2m\sqrt{(\sigma\Delta_M - \Delta_E)^2}}/\hbar$ will be imaginary for all values of Δ_E. This leads to $G_{AP} \to 0$ and to TMR = 100% for $-h \leq \Delta_E \leq h$. The predicted result indicates that a junction with a 100% TMR could easily be realized by setting $E = h = U$ in the regime of $|\Delta_E| \leq h$.

Finally, we show that when the Fermi energy E is very large, spin polarization and magnetoresistance of the junction may go to zero (see Figs. 8(a) and 8(b)). This is due to the fact that when the energy of the electron is very large, the difference in wave vector of electrons with spin-up and spin-down is very small. The large difference in behavior of S_P in the P-junction and AP-junction is found for E being small (see Fig. 8(a)). In addition, large S_P and TMR occur when the magnitude of E is comparable with h. The very large oscillation of TMR is predicted in the case of $\Delta_E \neq 0$. It may be said that

strong $S_{\rm P}$ and TMR may be achieved by using the condition of E being comparable with the net energy gap of the electron in the barrier.

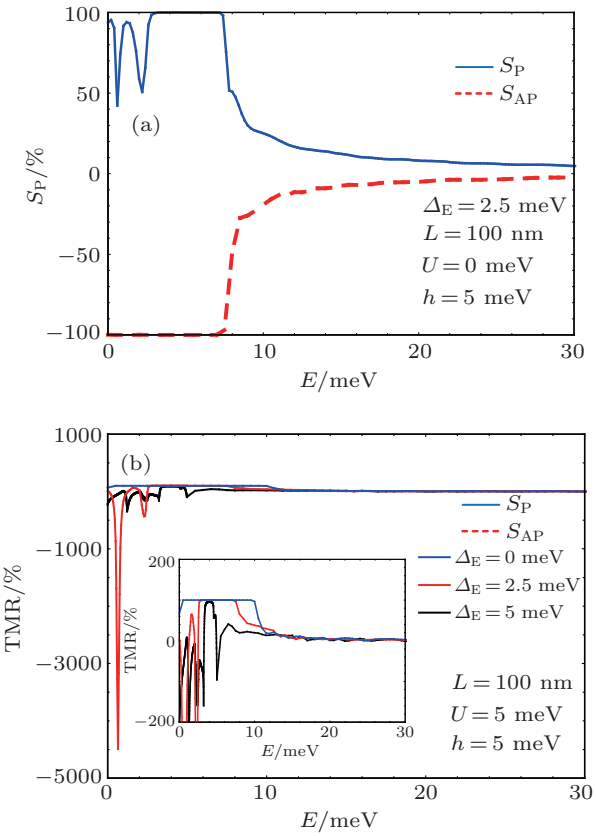


Fig. 8. (color online) Plot of spin-magnetic effect as a function of Fermi energy E. (a) Spin polarization $S_{\rm P}$ and (b) tunneling magnetoresistance TMR. There is no magnetic effect for large Fermi energy E.

6. Summary and conclusion

We have investigated the spin and magnetotransport properties of an AB-stacked bilayer graphene junction, which has a ferromagnetic-gated control barrier. The ferromagnetism in bilayer graphene can be induced by the proximity effect. The exchange fields in top and bottom layers can be either parallel (P) or antiparallel (AP). In this work, we have focused on the effect of an exchange-field-induced spin-dependent gap, which occurs only in the AP-junctions. It was found that, the AP-junction leads to several interesting results, which are important for spintronic applications such as the perfect spin filter where the perfect switching of spin polarization can be achieved by reversing the electric field. The junction under study also exhibits a giant tunneling magneto-resistance (a TMR of 100%). It was shown that the interesting behaviors occur because the energy dispersion relationship for the carriers in bilayer graphene acquires a spin-dependent gap. The gap is induced by a mismatch of exchange energy in the top and bottom layers. This work reveals the potential of bilayer graphene to be useful for applications in the area of spintronics.

Appendix A

The 4-component-Hamiltonian describing the motion of electrons in bilayer graphene, in which the top and bottom layers have potentials of V_1 and V_2 respectively, may be given by

$$E\begin{pmatrix}\varphi_{\rm A1}\\ \varphi_{\rm B1}\\ \varphi_{\rm A2}\\ \varphi_{\rm B2}\end{pmatrix}=\begin{pmatrix}V_1 & \hat{\pi}^* & 0 & 0\\ \hat{\pi} & V_1 & t & 0\\ 0 & t & V_2 & \hat{\pi}^*\\ 0 & 0 & \hat{\pi} & V_2\end{pmatrix}\begin{pmatrix}\varphi_{\rm A1}\\ \varphi_{\rm B1}\\ \varphi_{\rm A2}\\ \varphi_{\rm B2}\end{pmatrix}, \tag{A1}$$

where $\pi^*=\hbar v_{\rm F}(\hat{k}_x-{\rm i}\hat{k}_y)$ with $\hat{k}_{x(y)}=-{\rm i}\partial_{x(y)}$. The $\varphi_{\rm A1(2)}$ and $\varphi_{\rm B1(2)}$ are wave states of electrons in the A-sublattice for the top (bottom) layer and in the B-sublattice for the top (bottom) layer, respectively,

$$(V_1-E)\varphi_{\rm A1}+\hat{\pi}^*\varphi_{\rm B1}=0, \tag{A2}$$

$$\hat{\pi}\varphi_{\rm A1}+(V_1-E)\varphi_{\rm B1}+t\varphi_{\rm A2}=0, \tag{A3}$$

$$t\varphi_{\rm B1}+(V_2-E)\varphi_{\rm A2}+\hat{\pi}^*\varphi_{\rm B2}=0, \tag{A4}$$

$$\hat{\pi}\varphi_{\rm A2}+(V_2-E)\varphi_{\rm B2}=0. \tag{A5}$$

By using Eqs. (A3) and (A4), we obtain the components on the dimer sites $\varphi_{\rm B1}$ and $\varphi_{\rm A2}$ being respectively given of the forms

$$\varphi_{\rm B1}=-\frac{\hat{\pi}^*}{t\beta}\varphi_{\rm B2}+\frac{(V_2-E)\hat{\pi}}{t^2\beta}\varphi_{\rm A1}, \tag{A6}$$

$$\varphi_{\rm A2}=\frac{(V_2-E)\hat{\pi}^*}{t^2\beta}\varphi_{\rm B2}-\frac{\hat{\pi}}{t\beta}\varphi_{\rm A1}, \tag{A7}$$

where

$$\beta=\left(1-\frac{(V_2-E)(V_1-E)}{t^2}\right).$$

At the low energy limit, we may assume that $|V_2-E|\ll t$, $|V_1-E|\ll t$, and $|\pi|\ll t$ to obtain $\beta\to 1$. To ingore smaller terms related to $1/t^2$, equations (A6) and (A7) may be reduced into the forms

$$\varphi_{\rm B1}\cong-\frac{\hat{\pi}^*}{t}\varphi_{\rm B2},\qquad \varphi_{\rm A2}\cong-\frac{\hat{\pi}}{t}\varphi_{\rm A1}. \tag{A8}$$

Substituting Eq. (A8) into Eqs. (A1) and (A5), we thus obtain the effective two-component-Hamiltonian for bilayer graphene used in our work as obtained by

$$E\begin{pmatrix}\varphi_{\rm A1}\\ \varphi_{\rm B2}\end{pmatrix}=\begin{pmatrix}V_1 & -\frac{\hbar^2v_{\rm F}^2}{t}\left(\hat{k}_x-{\rm i}\hat{k}_y\right)^2\\ -\frac{\hbar^2v_{\rm F}^2}{t}\left(\hat{k}_x+{\rm i}\hat{k}_y\right)^2 & V_2\end{pmatrix}\begin{pmatrix}\varphi_{\rm A1}\\ \varphi_{\rm B2}\end{pmatrix}. \tag{A9}$$

In the P-junction, equation (2) can be described by setting $V_1=eE_zd-\sigma h+U$ and $V_2=-eE_zd-\sigma h+U$. In addition, in the AP-junction, equation (3) is given by setting $V_1=eE_zd-\sigma h+U$ and $V_2=-eE_zd+\sigma h+U$. In the normal region, equation (4) is described by setting $V_1=V_2=0$.

References

[1] Novoselov K S, Geim A K, Morozov S V, Jiang D, Zhang Y, Dubonos S V, Grigorieva I V and Firsov A A 2004 *Science* **306** 666

[2] Lin Y M, Dimitrakopoulos C, Jenkins K A, Farmer D B, Chiu H Y, Grill A and Avouris Ph 2010 *Science* **327** 662

[3] Schwierz F 2010 *Nat. Nanotechnol.* **5** 487

[4] Kheirabadi N, Shafiekhani A and Fathipour M 2014 *Superlatt. Microstruct.* **74** 123

[5] Geim A K and Novoselov K S 2007 *Nat. Mater.* **6** 183

[6] Katsnelson M I and Novoselov K S 2007 *Solid State Commun.* **143** 3

[7] Stander N, Huard B and Goldhaber-Gordon D 2009 *Phys. Rev. Lett.* **102** 026807

[8] Haugen H, Huertas-Hernando D and Brataas A 2008 *Phys. Rev. B* **77** 115406

[9] Swartz A G, Odenthal P M, Hao Y, Ruoff R S and Kawakami R K 2012 *ACS Nano* **6** 10063

[10] Cobas E, Friedman A L, van't Erve O M J, Robinson J T and Jonker B T 2012 *Nano Lett.* **12** 3000

[11] Yang H X, Hallal A, Terrade D, Waintal X, Roche S and Chshiev M 2013 *Phys. Rev. Lett.* **110** 046603

[12] Wang Z, Tang C, Sachs R, Barlas Y and Shi J 2015 *Phys. Rev. Lett.* **114** 016603

[13] Park J H and Lee H J 2014 *Phys. Rev. B* **89** 165417

[14] Soodchomshoma B, Tanga I M and Hoonsawata R 2009 *Physica E* **41** 1310

[15] Bai J, Cheng R, Xiu F, Liao L, Wang M, Shailos A, Wang K L, Huang Y and Duan V 2010 *Nat. Nanotechnol.* **5** 655

[16] Song Y and Dai G 2015 *Appl. Phys. Lett.* **106** 223104

[17] Zhang Y T, Jiang H, Sun Q F and Xie X C 2010 *Phys. Rev. B* **81** 165404

[18] Soodchomshom B and Chantngarm P 2011 *J. Supercond. Nov. Magn.* **24** 1885

[19] Fujita T, Jalil M B A and Tan S G 2010 *Appl. Phys. Lett.* **97** 043508

[20] Grujić M M, Tadić M Z and Peeters F M 2014 *Phys. Rev. Lett.* **113** 046601

[21] Castro N A H, Guinea F, Peres N M R, Novoselov K S and Geim A K 2009 *Rev. Mod. Phys.* **81** 109

[22] Zhang Y, Tang T T, Girit C, Hao Z, Martin M C, Zettl A, Crommie M F, Shen Y and Wang F 2009 *Nature* **459** 820

[23] Katsnelson M I, Novoselov K S and Geim A K 2006 *Nat. Phys.* **2** 620

[24] Derakhshan V and Cheraghchi H 2014 *J. Magn. Magn. Mater.* **357** 29

[25] Semenov Y G, Zavada J M and Kim K W 2008 *Phys. Rev. B* **77** 235415

[26] Cheraghchi H and Adinehvand F 2012 *J. Phys. Condens. Matter* **24** 045303

[27] Castro E V, López-Sancho M P and Vozmediano M A H 2011 *Phys. Rev. B* **84** 075432

[28] Michetti P and Recher P 2011 *Phys. Rev. B* **84** 125438

[29] Castro E V, Peres N M R, Stauber T and Silva N A P 2008 *Phys. Rev. Lett.* **100** 186803

[30] Lee K, Fallahazad B, Xue J, Dillen D C, Kim K, Taniguchi T, Watanabe K and Tutuc E 2014 *Science* **345** 58

[31] Hung N V, Bournel A and Dollfus P 2011 *J. Appl. Phys.* **109** 073717

[32] Yokoyama T 2008 *Phys. Rev. B* **77** 073413

[33] McCann E and Fal'ko V I 2006 *Phys. Rev. Lett.* **96** 086805

[34] Landauer R 1957 *IBM J. Res. Dev.* **1** 223